Materials Science & Engineering A 916 (2024) 147374

Contents lists available at ScienceDirect

Materials Science & Engineering A

journal homepage: www.elsevier.com/locate/msea

Enhanced cryogenic mechanical properties of heterostructured CrCoNi multicomponent alloy: Insights from *in-situ* neutron diffraction

Muhammad Naeem [a], Ricardo J. Sánchez Cruz [b], Miguel A. Esquivel Neri [b], Yuemin Ma [c], Vicente Amigó Borrás [d], Gonzalo González [e], Alexander J. Knowles [a], Wu Gong [f], Stefanus Harjo [f], Yuntian T. Zhu [g], Xun-Li Wang [c,h], Liliana Romero-Resendiz [a,b,i,*]

[a] School of Metallurgy and Materials, University of Birmingham, Birmingham, B15 2TT, UK
[b] Facultad de Química, Departamento de Ingeniería Metalúrgica, Universidad Nacional Autónoma de México, Mexico City, 04510, Mexico
[c] Department of Physics and Center for Neutron Scattering, City University of Hong Kong, Kowloon, Hong Kong
[d] Universitat Politècnica de València, Instituto de Tecnología de Materiales, Camino de Vera S/n, 46022, Valencia, Spain
[e] Instituto de Investigaciones en Materiales, Universidad Nacional Autónoma de México, Circuito Exterior S/n, Cd. Universitaria, A. P. 70-360, Coyoacán, C.P. 04510, Mexico
[f] J-PARC Center, Japan Atomic Energy Agency, 2-4 Shirakata, Tokai, Naka, Ibaraki, 319-1195, Japan
[g] Department of Materials Science and Engineering, City University of Hong Kong, Kowloon, Hong Kong
[h] Hong Kong Institute for Advanced Study, City University of Hong Kong, Tat Chee Avenue, Kowloon, Hong Kong
[i] Department of Design and Engineering, Faculty of Science and Technology, Bournemouth University, Poole, Dorset, BH12 5BB, UK

ARTICLE INFO

Keywords:
Heterostructured material
Medium-/high-entropy alloy
Mechanical properties
Cryogenic deformation
In situ testing

ABSTRACT

Heterostructured materials (HSMs) has been shown to improve the strength-ductility trade-off of conventional alloys but their cryogenic performance has not been studied during real-time deformation. We investigated heterostructured CrCoNi medium-entropy alloy by in-situ neutron diffraction at cryogenic (77 K) and room (293 K) temperatures. The significant mechanical mismatch at interfaces between fine and coarse grains, due to pronounced grain size disparity, resulted in exceptional yield strength of 918 MPa at 293 K. The yield strength further increased to 1244 MPa at 77 K with an excellent uniform elongation of 34 %. The exceptional strength–ductility combination at 77 K can be attributed to enhanced geometrically necessary dislocation pile-up density boosted from high-mechanical mismatch interfaces, as well as higher planar faults, and martensitic phase transformation. Comparison with homogenous counterparts demonstrates the potential of HSMs as a new strategy to improve the mechanical performance of different materials, including medium-/high-entropy alloys for cryogenic applications.

1. Introduction

Heterostructured materials (HSMs) are characterized by the coexistence of heterogeneous zones, which lead to a significant mechanical mismatch at the hetero-zone interfaces, for example, coarse- and fine-grained regions giving soft and hard zones, respectively [1,2]. Upon subjecting to stress, soft zones start deforming before the hard ones and geometrically necessary dislocations (GNDs) form near the hetero-zone interfaces to accommodate the mechanical incompatibility. Planar slip is the key factor that encourages GNDs to pile-up against hetero-zone interfaces, generating long-range back stresses that enhance the soft region's strengthening. In response, long-range forward stresses are developed at the hard regions, enhancing their strain hardening capability. The synergistic contribution of forward and back stresses is known as hetero-deformation-induced (HDI) stress, and it leads to better strength–ductility trade-off [3,4]. The efficiency of HDI strengthening and strain hardening can be anticipated to be affected by conditions that limit dislocation mobility and their interactions with interfaces. However, the real-time response of HSMs to cryogenic temperatures has never been investigated by in-situ deformation. These insights are crucial for cryogenic applications of alloys with outstanding strengthening and ductility for space exploration, storage and transportation systems, natural resources extraction at poles, hydrogen economy, superconducting magnets, food processing, etc.

* Corresponding author. Department of Design and Engineering, Faculty of Science and Technology, Bournemouth University, Poole, Dorset, BH12 5BB, UK.
E-mail address: lromeroresendiz@bournemouth.ac.uk (L. Romero-Resendiz).

https://doi.org/10.1016/j.msea.2024.147374
Received 30 June 2024; Received in revised form 29 August 2024; Accepted 7 October 2024
Available online 9 October 2024

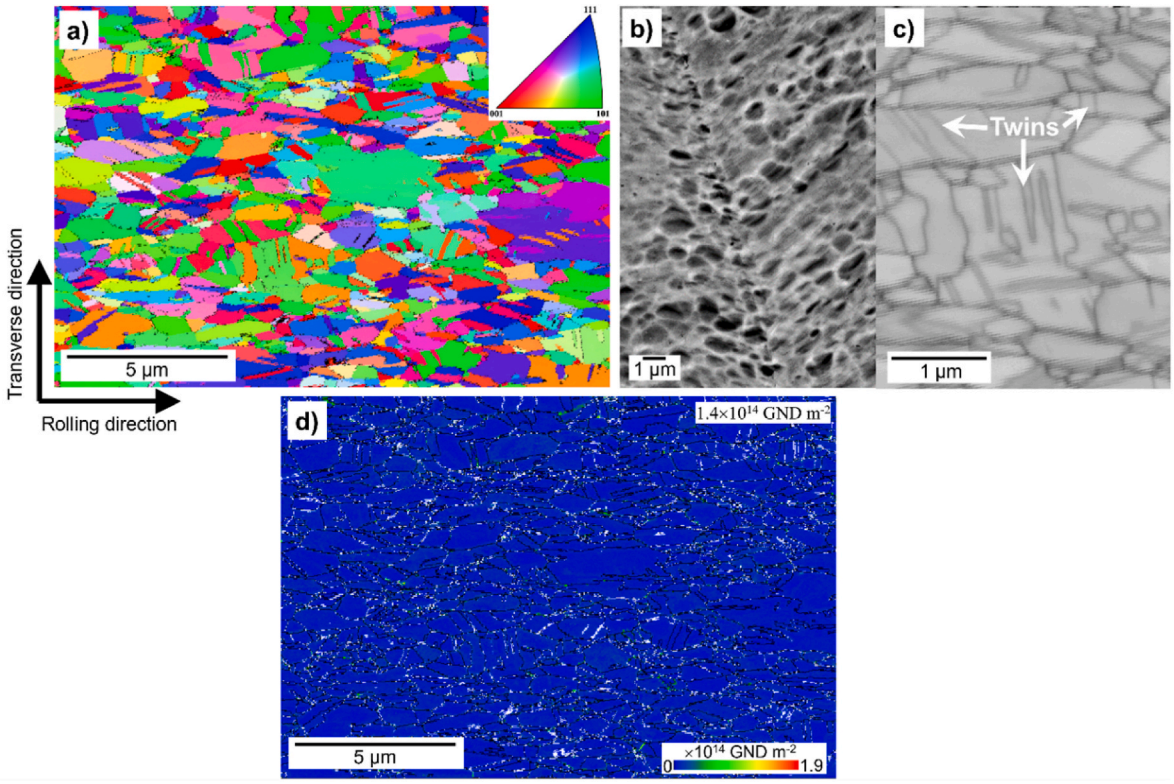

Fig. 1. Microstructural features of the undeformed heterostructured CrCoNi alloy. (a) EBSD inverse pole figure along the rolling plane, (b) SEM secondary electron micrograph showing abundant ultrafine and nanometric grains, (c) high magnification band contrast map showing twins, and (d) the GND map.

An alloy system that can ensure the dominance of planar slip at low temperatures can demonstrate the temperature-dependence of the strength–ductility trade-off of HSMs. Low stacking fault energy (SFE) and short-range order (SRO) are among the key parameters that promote planar slip as they make it difficult for two partial dislocations to combine [5]. The equiatomic CrCoNi medium-entropy alloy is an ideal candidate to form heterostructure due to its low SFE (22 mJ m^{-2} [6]) and SRO [7–9] that encourage planar slip [10–12]. Recently, in-situ deformation has been employed to explore the mechanical behavior, including the role of planar faults and the stacking fault-driven phase transformation in the CrCoNi alloy at low temperatures [12–14]. However, those studies were performed on homogeneous CrCoNi. The formation of different defects has also been shown in CrCoNi with hetero-zones [11,15–17], but by ex-situ and post-mortem microscopy analysis. Moreover, their defect densities have not been quantified. This work is the first approach to quantify and provide real-time defect evolution of a heterostructured multicomponent alloy under cryogenic conditions. We performed in-situ tensile testing with neutron diffraction to track defect evolution during uniaxial deformation at cryogenic (77 K) and room (293 K) temperatures in a heterostructured CrCoNi multicomponent alloy.

2. Material and methods

Equiatomic CrCoNi alloy was produced by arc melting and suction casting using raw elements with a purity of >99.5 %. The cast alloy was homogenized at 1200 °C for 24 h and then quenched in water. An 80 % reduction in thickness by cold rolling followed by a partial recrystallization at 750 °C for 600 s and then water-quenching was applied to produce HSM consisting of coarse-grained regions surrounded by ultrafine-grained regions. Electron backscatter diffraction (EBSD) was carried out with an HKL Nordlys EBSD detector at 15 kV adapted to a Zeiss Auriga scanning electron microscope (SEM) with a step size of 0.07 μm for grain size distribution analyses and 1 μm for overall micrographs. Grain size quantification was performed by the AZtecCrystal software by considering only indexed points and a misorientation threshold of 10°. The twin boundaries were excluded from grain size statistics based on the theoretical 60° misorientation with <111> axis [18]. A grain orientation spread between 1° and 2° was used to differentiate recrystallized grains with low internal strain from deformed unrecrystallized grains. GND estimation was carried out by the kernel average misorientation, i.e., misorientation around a measurement point with respect to its nearest neighbors, using the AZtecCrystal software. Tensile samples with loading axis parallel to the rolling direction were fabricated. Gauge dimensions of 0.5 × 3.7 × 25 (thickness × width × length, all in mm) were used for in-situ neutron diffraction at the TAKUMI beamline of the Materials and Life Science Experimental Facility, Japan Proton Accelerator Research Complex (J-PARC Center). Uniaxial tensile tests were performed at a strain rate of 2.67 × 10^{-5} s^{-1}. The diffraction data was obtained continuously throughout the deformation at 77 and 293 K. Additionally, defects observation of the sample deformed at 77 K was performed with transmission electron microscope (TEM) in a JEOL ARM200F.

3. Results and discussion

The microstructural characteristics of CrCoNi alloy before deformation are shown in Fig. 1. Each color in Fig. 1a represents a different crystal orientation as referenced in the inserted standard inverse pole figure. A nearly random crystallographic orientation is suggested from the non-preferential color in Fig. 1a and Figs. S1a and b, and confirmed by the similar trends between the theoretical Mackenzie for randomly oriented face-centered cubic (FCC) crystal structures and the experimental random pair misorientation distributions in Fig. S1c [19]. Fig. 1a shows a microstructure consisting of non-equiaxed micrometric recrystallized (RG > 1 μm, ~6 %) and ultrafine (0.1 μm > UFG < 1 μm, ~76 %) grain colonies surrounded by nanometric grains (NG < 0.1 μm, ~18 %, Fig. 1b). Twins and a GND density of 1.4 × 10^{14} m^{-2} – induced by cold

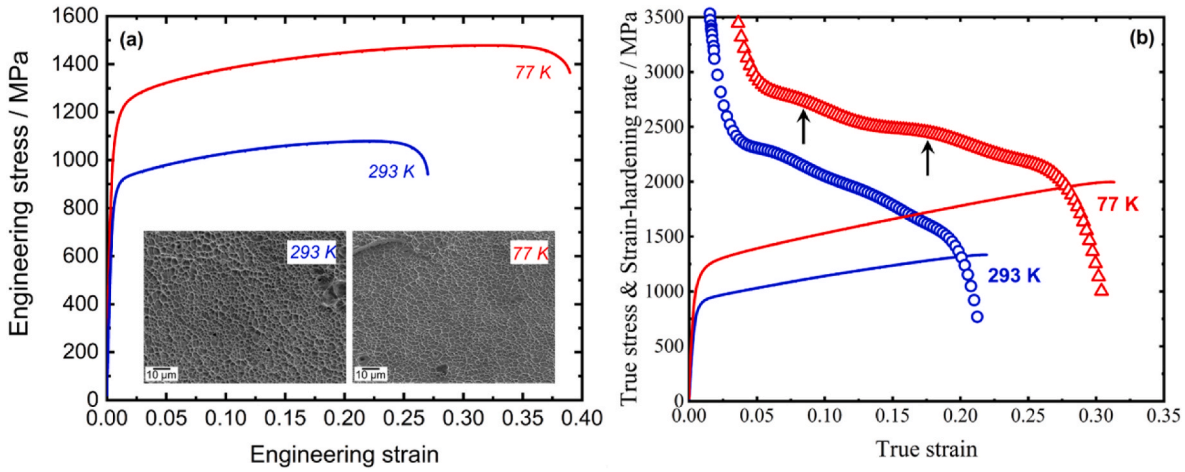

Fig. 2. Tensile deformation behavior of heterostructured CrCoNi alloy. (a) Engineering stress-strain curves, and (b) the strain hardening rate superimposed on the true stress-strain curves at 293 and 77 K. The insets in (a) show SEM fractographs after fracture.

Table 1
The comparison of yield strength (σ_Y), ultimate tensile strength (σ_{UTS}), elongation till fracture (ε_f) and uniform elongation (ε_u) at 293 and 77 K. The elastic modulus (E) and the lattice parameter before deformation (a_0) are also listed.

Temperature/ K	σ_Y/MPa	σ_{UTS}/MPa	ε_f/%	ε_u/%	E/ GPa	a_0/Å
293	918 ± 22	1079 ± 25	27 ± 0.6	23.1 ± 0.5	249 ± 6	3.56314
77	1244 ± 28	1478 ± 41	39 ± 1.2	33.6 ± 1.0	256 ± 8	3.55542

rolling and remaining after the partial recrystallization – are observed in Fig. 1c and d. The neighbor pair distribution in Fig. S1c confirms twinning, as indicated by the peak with a high relative frequency of 0.53 at a misorientation of approximately 60°. This corresponds to the Σ3 coincidence site lattice orientations, characterized by a 60° <111> twist boundary resulting from twinning [18].

Fig. 2 shows tensile stress-strain and strain hardening rate curves for the heterostructured CrCoNi alloy. Table 1 lists comparison of mechanical properties at 293 and 77 K. The alloy possesses a high yield strength (σ_Y) of 918 MPa, an ultimate tensile strength (σ_{UTS}) of 1079 MPa, fracture strain (ε_f) of 27 %, and uniform strain (ε_u) of 23.1 % at

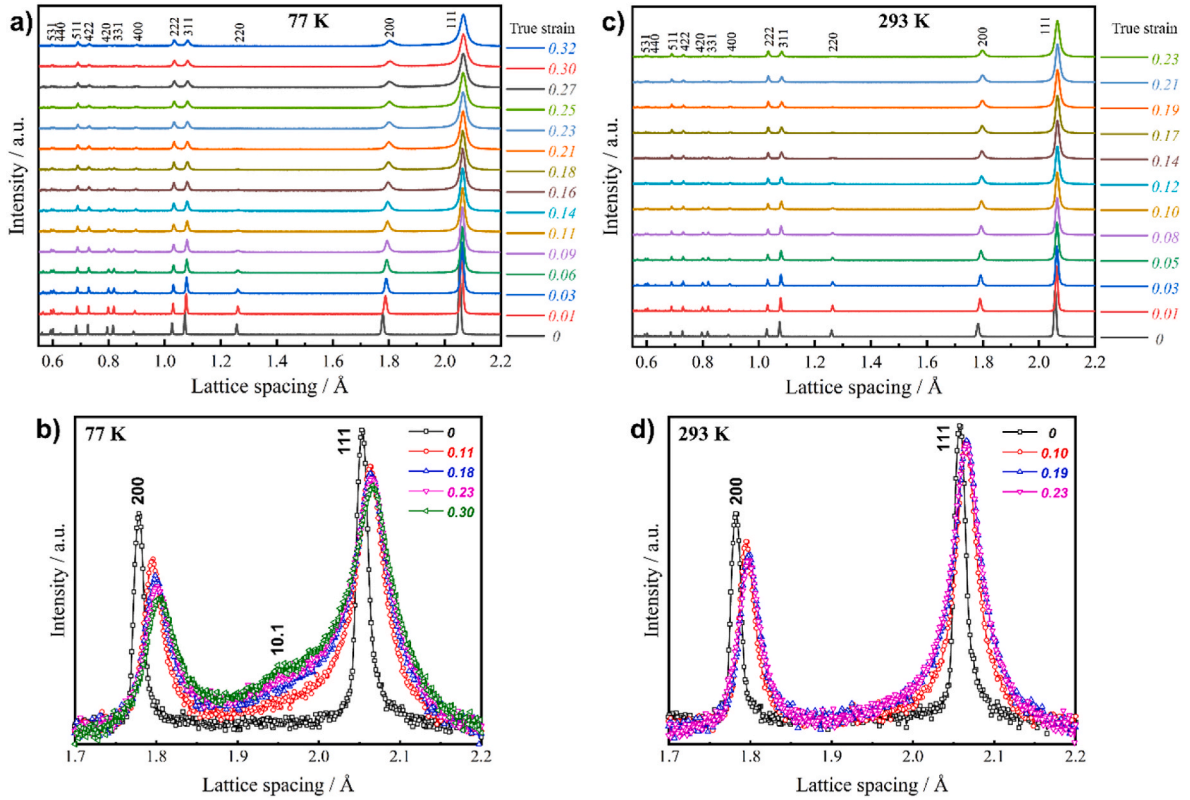

Fig. 3. Neutron diffractograms with true deformation strains showing the structure evolution at (a,b) 77 K and (c,d) 293 K. Plots in (b,d) show zoomed-in of selected patterns in the range 1.7–2.2 Å, with intensity plotted in log-scale, to emphasize in (b) the profile asymmetry and the emergence of HCP (10.1) peak at 77 K and in (d) lack of the hcp formation at 293 K.

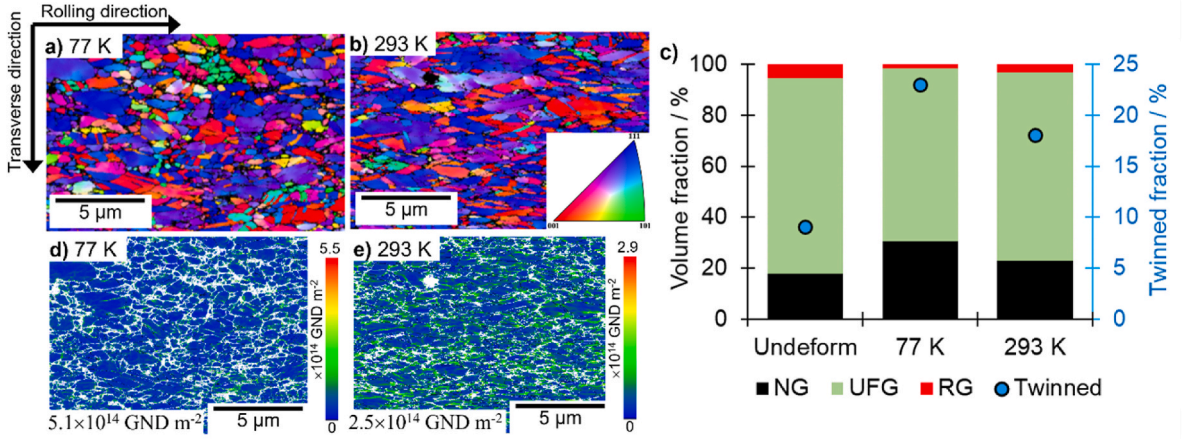

Fig. 4. Microstructural evolution of deformed heterostructured CrCoNi at 77 and 293 K. (a,b) Inverse pole figures along the rolling plane, (c) grain size distribution (NG = nanograins, UFG = ultrafine grains, and RG = recrystallized grains) and twinned grain fractions, and (d,e) GND maps with GND density for both temperatures.

293 K. At 77 K, all these mechanical properties are enhanced significantly, with σ_Y, σ_{UTS}, ε_f and ε_u reaching 1244 MPa, 1478 MPa, 39 % and 33.6 %, respectively. The SEM micrographs (as insert of Fig. 2a) shows the fractured surface at 293 and 77 K. Both samples present a ductile fracture behavior given by the formation of homogeneously distributed voids and dimples. Fig. 2b depicts strain hardening rates superimposed on true stress-strain curves. The sample at 77 K exhibits a high strain hardening rate of ~2850 MPa in the early-stage of deformation. The rate decreased to ~2000 MPa during subsequent straining up to a true strain of ~0.27 and at the onset of necking. The drop in the strain hardening is not linear at 77 K. The two regions with stable rate were observed (between a true strain of ~0.08 and ~0.16, as indicated by the arrows in Fig. 2b), which will be later linked to the activation of sequential strain hardening mechanisms. In contrast, the strain hardening rate at 293 K is lower throughout the entire deformation process; it starts at ~2350 MPa and continuously decreases to ~1350 MPa until necking. As expected, the lattice parameter (a_0) decreased at 77 K due to thermal contraction while the elastic modulus (E) increased with decreasing temperature indicating a higher stiffness at 77 K (Table 1).

The structure evolution during different stages of deformation can be observed from neutron diffraction patterns in Fig. 3. The lattice spacing increased as a result of deformation at both temperatures. The influence of planar faults towards the peak asymmetry [12,20] becomes evident from true strain of ~0.11 in the sample deformed at 77 K (Fig. 3b). This ultimately leads to the martensitic transformation from the overlapping of stacking faults into hexagonal close-packed (HCP) phase [12,14, 21–24]. The formation of an HCP (10.1) peak hump at 77 K in Fig. 3a and b is the result of such mechanism. The martensitic transformation was not observed in the sample deformed at 293 K, where the peaks remain relatively symmetrical until the end (Fig. 3d).

Fig. 4a and b shows the EBSD microstructure of the heterostructured CrCoNi alloy after deformation at 77 and 293 K. As evident from the inverse pole figures, a preferential orientation of crystals towards <111> and <001> was formed during deformation along the rolling plane and confirmed by misorientation distributions that do not follow the theoretical random orientation for FCC structures [19] (Fig. S2). However, the transverse and normal planes did not show a significant crystallographic orientation evolution with respect to the undeformed condition in Fig. 1 and Fig. S1. This is because of the uniaxial nature of the tensile test, where the deformation mainly influences the loading plane (which in this case coincides with the rolling plane) causing the crystal axes near the (101) to rotate towards the (111) or the (100), thus significantly increasing their intensity along the loading direction but not for the transversal direction in FCC systems [25]. After fracture, the sample deformed at 77 K had higher NGs and lower number density of UFGs and RGs than the sample deformed at 293 K (Fig. 4c). Moreover,

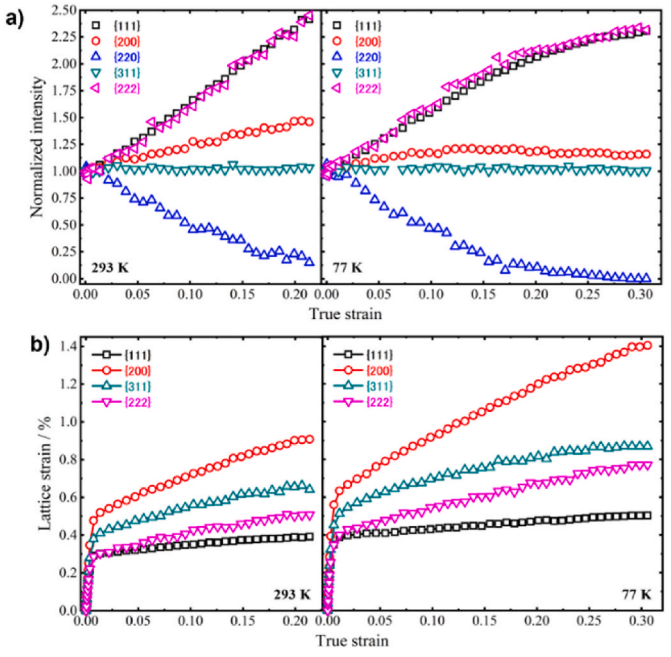

Fig. 5. (a) Normalized integrated intensity indicating texture development and (b) lattice strain evolution along different lattice planes at 293 and 77 K.

the sample at 77 K also had higher fraction of twinned grains (23 %) than at 293 K (17 %), indicating a higher planar fault activity at lower temperature. The increasing neighbor pair misorientation peak near 60° (Fig. S2) also indicates a higher twin fraction at 77 K than at 293 K [26]. The strain gradient near the hetero-zone interfaces given by different order of grain sizes triggered a higher density of GNDs to accommodate the strain [1]. As indicated in Fig. 4d and e, the GND density increased to 2.5 and 5.1 × 10^{14} GND m^{-2} at 293 and 77 K with respect to the undeformed condition (1.4 × 10^{14} GND m^{-2}, Fig. 1d).

In general, the samples showed a microstructural evolution mainly described by grain refinement with a preferred crystallographic orientation towards <111> and <100> in the rolling direction with deformation at both 293 and 77 K. The different crystallographic orientation generated at both temperatures can be further observed by the normalized intensity of the crystallographic planes as a function of the true strain (Fig. 5a). While all the planes follow a linear tendency at 293 K which is typical for deformation by dislocation slip, their trend slowed down after a true strain of ~0.16 at 77 K. This may indicate the

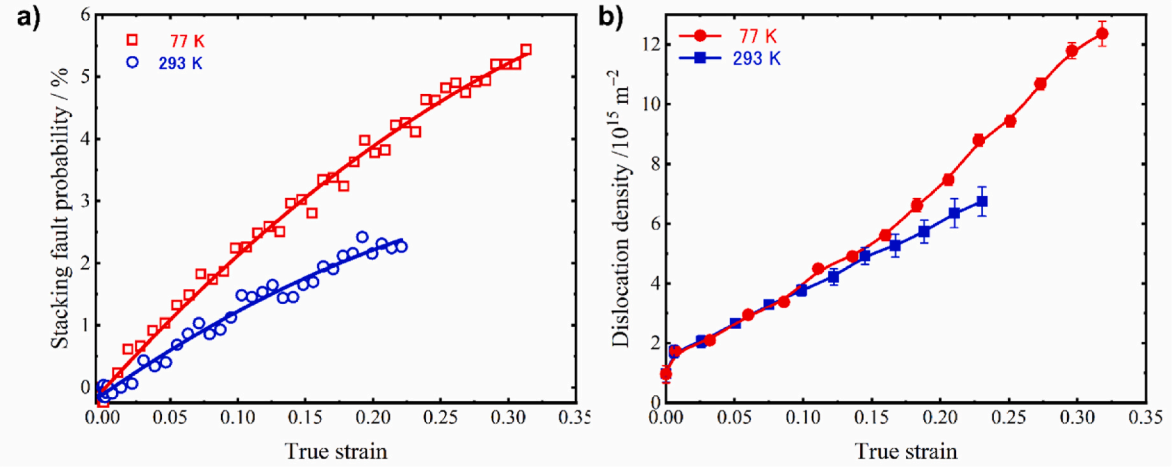

Fig. 6. Defect evolution with deformation at 293 and 77 K in the form of (a) stacking fault probability and (b) dislocation density.

activation of a different deformation mechanism (martensitic transformation, Fig. 3b) which also coincides with the strain hardening rate stabilization indicated in Fig. 2b. This effect is evident from the asymmetrical peaks and formation of HCP phase (Fig. 3b), which indicate significant stacking fault activity [11,12]. The lattice strain difference between the same family of planes, i.e., {111} and {222} at both temperatures (Fig. 5b), suggests the development of stacking fault probability (SFP) [27]. SFP is the tendency of a material to form stacking faults and can be evidenced by the accumulation of stacking faults that cause the relative shift of the two aforementioned crystallographic planes. This difference can be used to estimate SFP, as shown in Fig. 6a. The SFP at 77 K (~5.3 %) is more than twice that of 293 K (~2.4 %), explaining the lack of HCP formation at 293 K (Fig. 3b) due to limited stacking faults to overlap. The higher SFP at low temperature may be related to the limited dislocation mobility that encourages the activation of alternative deformation mechanisms [20,28,29]. The higher SFP of the heterostructured CrCoNi alloys in this study compared to that of homogeneous CrCoNi alloys [12,14] is an indication of higher planar fault activity, i.e., lower SFE according to Eq. (1) [30].

$$\mathrm{SFE} = \frac{6.6a_0}{\pi\sqrt{3}}\left(\frac{2c_{44}}{c_{11}\text{-}c_{12}}\right)^{-0.37}\frac{\langle\varepsilon_{50}^2\rangle}{\mathrm{SFP}}\left(\frac{c_{44}+c_{11}\text{-}c_{12}}{3}\right) \qquad \text{Eq. (1)}$$

where a_0 is the lattice constant, c_{11}, c_{12} and c_{44} are the single crystal elastic constants, and $\langle\varepsilon_{50}^2\rangle$ is the mean square strain. The lower SFE of heterostructured CrCoNi may promote planar slip that encourages more GND pile-ups to accommodate the high strain gradient at interfaces, leading to higher HDI stress [1]. The higher SFP (Fig. 6a) agrees with the higher GND density at 77 K (Fig. 4d).

The abovementioned behavior can be explained by the dominance of planar slip at low temperature. Considering cross-slip is a thermally activated mechanism, the low temperatures can reduce the cross slip rate *r(T)* according to the Arrhenius equation (Eq. (2)) [31,32].

$$r(T) = \nu\, e^{-\frac{H_A}{T\,k_B}} \qquad \text{Eq. (2)}$$

where ν is the rate prefactor, H_A is the activation enthalpy, T is the absolute temperature, and k_B is the Boltzmann's constant. From analytical solutions, an increase of the energy barrier for cross slip is expected for lower SFE [31], creating more extended dislocation cores that hinder cross slip, facilitating planar slip [33]. This effect may be even stronger in concentrated alloys, like the multicomponent CrCoNi of this work, where the local atomic environment can significantly influence the SFE and act as a secondary barrier for dislocation motion by the increment of friction stress [13,34]. This phenomenon agrees with the high density of twin formation in the deformed CrCoNi (Fig. 4c). In addition to a more efficient formation of twins, stacking faults, and HDI stress, the improved strength of the heterostructured CrCoNi compared to its homogeneous counterparts (Fig. 7) is also explained by its higher dislocation density (Fig. 6b). The higher value of $\frac{d\rho}{d\varepsilon}$ suggests a reduced dynamic recovery due to dominant planar slip (over cross slip) in the heterostructured CrCoNi compared to the homogeneous counterparts. From Fig. 6b, heterostructured CrCoNi at 77 K (~ 25.3 to 37.2 × 10^{15} m^{-2}) and 293 K (~ 22.4 × 10^{15} m^{-2}) shows overall higher $\frac{d\rho}{d\varepsilon}$ than the homogeneous counterparts at 140 K (~ 19.7 × 1 0^{15} m^{-2}) and 293 K (~ 14.5 × 10^{15} m^{-2}) [12]. A change of $\frac{d\rho}{d\varepsilon}$ in the heterostructured CrCoNi at 77 K from a true strain of ~0.16 suggests faster dislocation density increment with a significant work hardening rate. This value of ~0.16 strain is in agreement with the second stable strain hardening rate region in Fig. 2b as well as occurrence of phase transformation at later deformation stages [12].

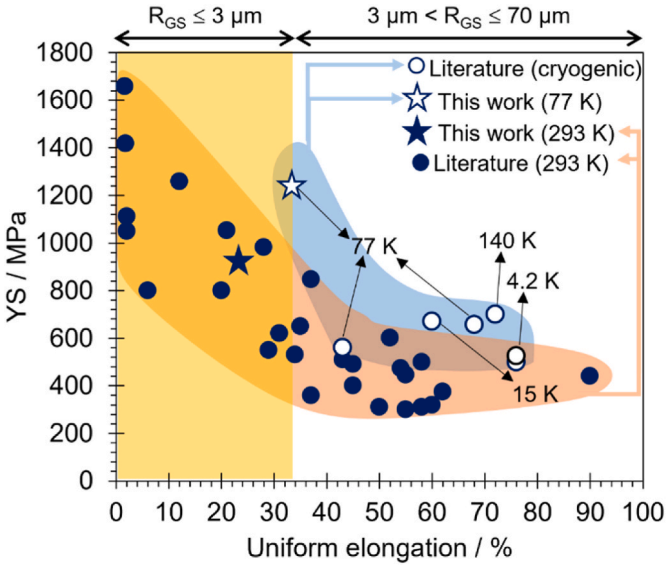

Fig. 7. Comparison of yield strength (YS) vs. uniform elongation among present and reported CrCoNi alloys with different ranges of grain size (R_{GS}) [6,11,12,14,15,35–40]. The cryogenic data points are shown in light blue with the specific temperatures marked, while the room temperature is indicated in dark blue. (For interpretation of the references to color in this figure legend, the reader is referred to the Web version of this article.)

The strengthening of the heterostructured CrCoNi alloy at 77 K

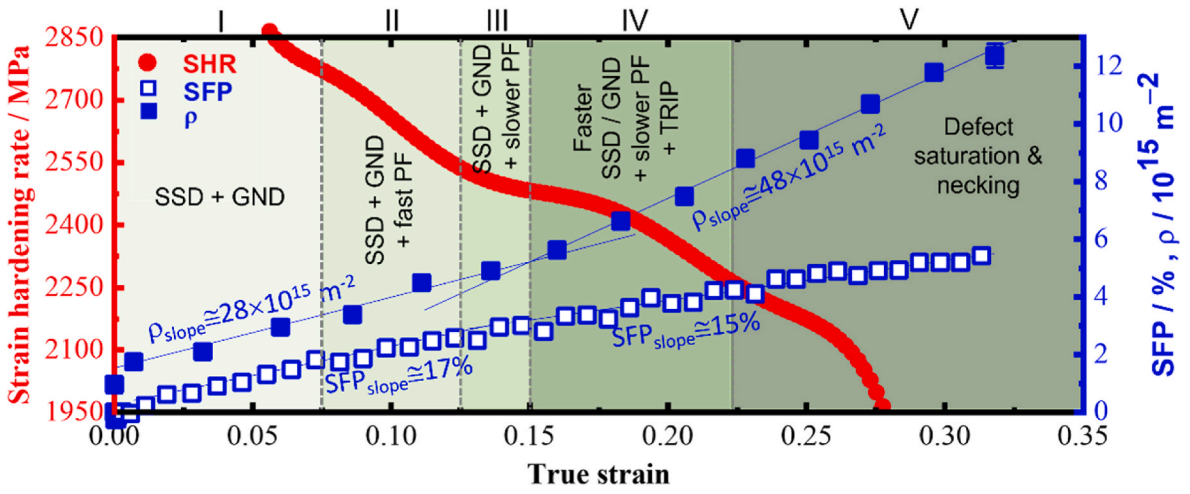

Fig. 8. Sequence for the activation of different deformation mechanisms for the heterostructured CrCoNi alloy at 77 K. The trends for strain hardening rate (SHR), stacking fault probability (SFP), and total dislocation density (ρ) are indicated as a function of true strain.

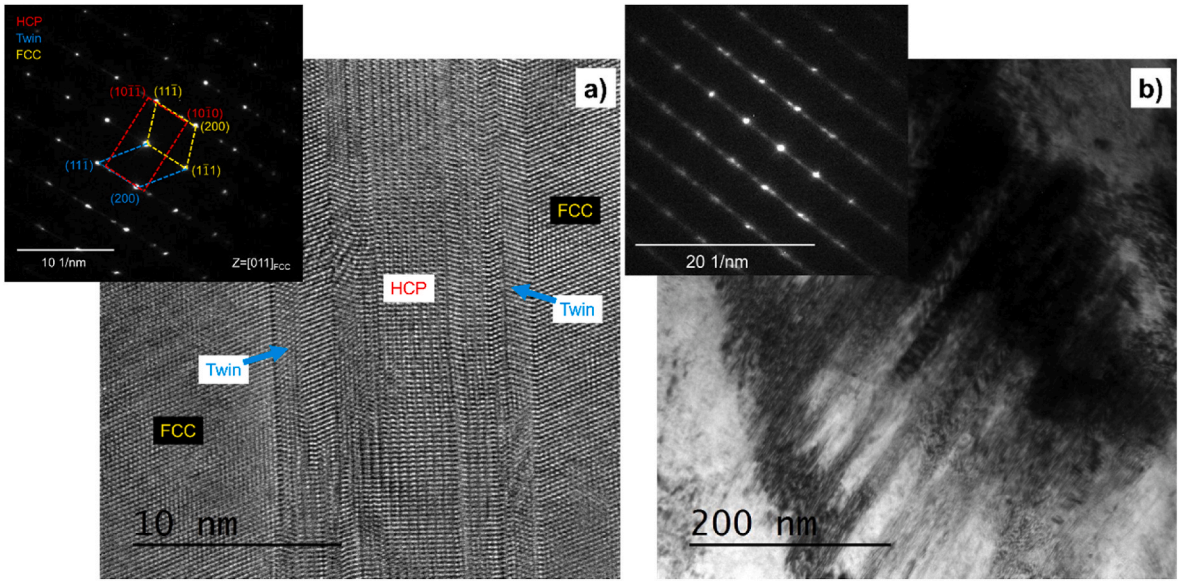

Fig. 9. TEM micrographs showing (a) twins, HCP-martensite and FCC-matrix phase, and (b) stacking faults, formed in the heterostructured CrCoNi deformed at 77 K. The selected area electron diffraction patterns display arrangement and streaks typical of (insert in a) twins, HCP and FCC phases, and (insert in b) stacking faults, respectively.

originates from multiple synergistic mechanisms activated sequentially in five stages indicated in Fig. 8. In stage I, the initial deformation starts at softer regions, before hard regions, and lead to GND piling up in the micrometric (RG and UFG) regions. Meanwhile, statistically stored dislocations (SSDs) are accumulated within grains by mutual trapping [41]; their quantity can be deduced from the difference between the total dislocation density (ρ) (Fig. 6b) and the GND density (Fig. 4c) [42]. Planar faults (PFs), including twins (Figs. S2 and 4c) and stacking faults, also start forming at stage I. TEM images in Fig. 9 also provide evidence of stacking faults and twins in the heterostructured CrCoNi alloy deformed at 77 K. The number density of these defects continue increasing during stage II, leading to the first strain hardening rate stable region (Fig. 2b). Stage III is characterized by a lower PF quantity shown by a decreasing SFP slope from 17 to 15 %, indicating a significant density of PFs has accumulated and overlapping to act as nucleation sites for FCC-to-HCP phase transformation during stage IV (Fig. 3b) [12,14]. The high-resolution TEM as well as the selected area electron diffraction pattern in Fig. 9a shows the HCP phase formation in heterostructed CrCoNi sample after deformation at 77 K. Transformation induced plasticity (TRIP), together with faster dislocation density increment, shown by increase in slope from ~28 to ~48 × 10^{15} m^{-2} in Fig. 8, led to the second strain hardening rate stable region in Fig. 2b. The defect saturation occurs in stage V and ultimately necking forms.

A comparison of the σ_Y *vs.* ε_U of reported (homogeneous and heterostructured) [6,11,12,14,15,35–40] and present heterostructured CrCoNi alloys tested at different temperatures is shown in Fig. 7. The superior strength–ductility trade-off of heterostructured materials comes from the synergy of multiple strengthening and strain hardening mechanisms, including GND pile-ups-driven HDI stress as well as solid solution, SSD accumulation, stacking faults, twinning, phase transformation, and grain boundaries. It should be remarked that other factors in the hetero-zones may also affect defect formation, such as local compositional gradients, different crystal structures, soft and hard region distributions, etc. The systematic study of those factors remains for future exploration.

4. Conclusions

We studied the deformation behavior of heterostructured CrCoNi medium-entropy alloy at room and cryogenic temperatures. The crucial role of GND density and stacking fault probability was found to be significantly higher at low temperature, indicating a propensity toward HDI stress, planar fault formation and phase transformation. The comparison with reported homogeneous CrCoNi alloys suggests that the existence of hetero-zones in the heterostructured CrCoNi alloy promotes a more efficient synergy of sequential deformation mechanisms that contribute to its better strength–ductility trade-off. The results emphasize the potential of heterostructured materials in applications requiring high strength and ductility, particularly at low temperatures.

CRediT authorship contribution statement

Muhammad Naeem: Writing – original draft, Visualization, Supervision, Project administration, Methodology, Investigation, Formal analysis, Conceptualization. **Ricardo J. Sánchez Cruz:** Methodology, Formal analysis. **Miguel A. Esquivel Neri:** Methodology, Formal analysis. **Yuemin Ma:** Writing – review & editing, Formal analysis. **Vicente Amigó Borrás:** Writing – review & editing, Methodology. **Gonzalo González:** Writing – review & editing, Validation. **Alexander J. Knowles:** Writing – review & editing, Validation. **Wu Gong:** Methodology. **Stefanus Harjo:** Writing – review & editing, Validation. **Yuntian T. Zhu:** Writing – review & editing, Validation. **Xun-Li Wang:** Writing – review & editing, Validation, Resources. **Liliana Romero-Resendiz:** Writing – original draft, Visualization, Resources, Methodology, Investigation, Funding acquisition, Formal analysis, Conceptualization.

Declaration of competing interest

The authors declare that they have no known competing financial interests or personal relationships that could have appeared to influence the work reported in this paper.

Acknowledgments

This work was supported by the Programa de Apoyo a la Investigación y el Posgrado (PAIP-50009223) of Universidad Nacional Autónoma de México, the Programa de Apoyo a Proyectos de Investigación e Innovación Tecnológica (PAPIIT-UNAM IA102724 and IN110124), and the Research Grants Council of Hong Kong Special Administrative Region (C1020-21G). M.N. acknowledges Asia-Oceania Neutron Scattering Association (AONSA) for the AONSA Young Research Fellowship (AONSA-YRF-2022). L.R-R. acknowledges the HORIZON EUROPE programme of research and innovation of the European Union evaluated under the Marie Sklodowska-Curie call and financed by UK Research and Innovation, grant agreement No EP/Y020545/1. X.L.W. thanks the Croucher Foundation for the Croucher Senior Research Fellowship (CityU 9509008). S.H. acknowledges the support from the MEXT Program: Data Creation and Utilization Type Material Research and Development (JPMXP1122684766). The neutron experiments at the Materials and Life Science Experimental Facility at J-PARC Center were conducted under the user program (proposal number 2022B0140).

Appendix A. Supplementary data

Supplementary data to this article can be found online at https://doi.org/10.1016/j.msea.2024.147374.

Data availability

Data will be made available on request.

References

[1] Y. Zhu, X. Wu, Heterostructured materials, Prog. Mater. Sci. 131 (2023) 101019, https://doi.org/10.1016/j.pmatsci.2022.101019.
[2] K. Edalati, A.Q. Ahmed, S. Akrami, K. Ameyama, V. Aptukov, R.N. Asfandiyarov, M. Ashida, V. Astanin, A. Bachmaier, V. Beloshenko, E.V. Bobruk, K. Bryła, J. M. Cabrera, A.P. Carvalho, N.Q. Chinh, I.-C. Choi, R. Chulist, J.M. Cubero-Sesin, G. Davdian, M. Demirtas, S. Divinski, K. Durst, J. Dvorak, P. Edalati, S. Emura, N. A. Enikeev, G. Faraji, R.B. Figueiredo, R. Floriano, M. Fouladvind, D. Fruchart, M. Fuji, H. Fujiwara, M. Gajdics, D. Gheorghe, Ł. Gondek, J.E. González-Hernández, A. Gornakova, T. Grosdidier, J. Gubicza, D. Gunderov, L. He, O. F. Higuera, S. Hirosawa, A. Hohenwarter, Z. Horita, J. Horky, Y. Huang, J. Huot, Y. Ikoma, T. Ishihara, Y. Ivanisenko, J. Jang, A.M. Jorge, M. Kawabata-Ota, M. Kawasaki, T. Khelfa, J. Kobayashi, L. Kommel, A. Korneva, P. Kral, N. Kudriashova, S. Kuramoto, T.G. Langdon, D.-H. Lee, V.I. Levitas, C. Li, H.-W. Li, Y. Li, Z. Li, H.-J. Lin, K.-D. Liss, Y. Liu, D.M.M. Cardona, K. Matsuda, A. Mazilkin, Y. Mine, H. Miyamoto, S.-C. Moon, M. Müller, J.A. Muñoz, M.Yu Murashkin, M. Naeem, M. Novelli, D. Olasz, R. Pippan, V.V. Popov, E.N. Popova, G. Purcek, P. de Rango, O. Renk, D. Retraint, Á. Révész, V. Roche, P. Rodriguez-Calvillo, L. Romero-Resendiz, X. Sauvage, T. Sawaguchi, H. Sena, H. Shahmir, X. Shi, V. Sklenicka, W. Skrotzki, N. Skryabina, F. Staab, B. Straumal, Z. Sun, M. Szczerba, Y. Takizawa, Y. Tang, R.Z. Valiev, A. Vozniak, A. Voznyak, B. Wang, J.T. Wang, G. Wilde, F. Zhang, M. Zhang, P. Zhang, J. Zhou, X. Zhu, Y.T. Zhu, Severe plastic deformation for producing Superfunctional ultrafine-grained and heterostructured materials: an interdisciplinary review, J. Alloys Compd. 1002 (2024) 174667, https://doi.org/10.1016/j.jallcom.2024.174667.
[3] Y. Zhu, K. Ameyama, P.M. Anderson, I.J. Beyerlein, H. Gao, H.S. Kim, E. Lavernia, S. Mathaudhu, H. Mughrabi, R.O. Ritchie, N. Tsuji, X. Zhang, X. Wu, Heterostructured materials: superior properties from hetero-zone interaction, Mater Res Lett 9 (2021) 1–31, https://doi.org/10.1080/21663831.2020.1796836.
[4] L. Romero-Resendiz, M. El-Tahawy, T. Zhang, M.C. Rossi, D.M. Marulanda-Cardona, T. Yang, V. Amigó-Borrás, Y. Huang, H. Mirzadeh, I.J. Beyerlein, J. C. Huang, T.G. Langdon, Y.T. Zhu, Heterostructured stainless steel: properties, current trends, and future perspectives, Mater Sci Eng R 150 (2022) 100691, https://doi.org/10.1016/j.mser.2022.100691.
[5] L. Romero-Resendiz, M. Naeem, Y.T. Zhu, Heterostructured materials by severe plastic deformation: overview and perspectives, Mater. Trans. 64 (2023) 2346–2360, https://doi.org/10.2320/matertrans.MT-MF2022010.
[6] G. Laplanche, A. Kostka, C. Reinhart, J. Hunfeld, G. Eggeler, E.P. George, Reasons for the superior mechanical properties of medium-entropy CrCoNi compared to high-entropy CrMnFeCoNi, Acta Mater. 128 (2017) 292–303, https://doi.org/10.1016/j.actamat.2017.02.036.
[7] F.X. Zhang, S. Zhao, K. Jin, H. Xue, G. Velisa, H. Bei, R. Huang, J.Y.P. Ko, D. C. Pagan, J.C. Neuefeind, W.J. Weber, Y. Zhang, Local structure and short-range order in a NiCoCr solid solution alloy, Phys. Rev. Lett. 118 (2017) 205501, https://doi.org/10.1103/PhysRevLett.118.205501.
[8] R. Zhang, S. Zhao, J. Ding, Y. Chong, T. Jia, C. Ophus, M. Asta, R.O. Ritchie, A. M. Minor, Short-range order and its impact on the CrCoNi medium-entropy alloy, Nature 581 (2020) 283–287, https://doi.org/10.1038/s41586-020-2275-z.
[9] B. Yin, S. Yoshida, N. Tsuji, W.A. Curtin, Yield strength and misfit volumes of NiCoCr and implications for short-range-order, Nat. Commun. 11 (2020) 2507, https://doi.org/10.1038/s41467-020-16083-1.
[10] M. Yang, D. Yan, F. Yuan, P. Jiang, E. Ma, X. Wu, Dynamically reinforced heterogeneous grain structure prolongs ductility in a medium-entropy alloy with gigapascal yield strength, Proc. Natl. Acad. Sci. U. S. A. 115 (2018) 7224–7229, https://doi.org/10.1073/pnas.1807817115.
[11] C.E. Slone, J. Miao, E.P. George, M.J. Mills, Achieving ultra-high strength and ductility in equiatomic CrCoNi with partially recrystallized microstructures, Acta Mater. 165 (2019) 496–507, https://doi.org/10.1016/j.actamat.2018.12.015.
[12] M. Naeem, H. Zhou, H. He, S. Harjo, T. Kawasaki, S. Lan, Z. Wu, Y. Zhu, X.-L. Wang, Martensitic transformation in CrCoNi medium-entropy alloy at cryogenic temperature, Appl. Phys. Lett. 119 (2021) 131901, https://doi.org/10.1063/5.0067268.
[13] Q. Ding, X. Fu, D. Chen, H. Bei, B. Gludovatz, J. Li, Z. Zhang, E.P. George, Q. Yu, T. Zhu, R.O. Ritchie, Real-time nanoscale observation of deformation mechanisms in CrCoNi-based medium- to high-entropy alloys at cryogenic temperatures, Mater. Today 25 (2019) 21–27, https://doi.org/10.1016/J.MATTOD.2019.03.001.
[14] H. He, M. Naeem, F. Zhang, Y. Zhao, S. Harjo, T. Kawasaki, B. Wang, X. Wu, S. Lan, Z. Wu, W. Yin, Y. Wu, Z. Lu, J.-J. Kai, C.-T. Liu, X.-L. Wang, Stacking Fault driven phase transformation in CrCoNi medium entropy alloy, Nano Lett. 21 (2021) 1419–1426, https://doi.org/10.1021/acs.nanolett.0c04244.
[15] P. Sathiyamoorthi, P. Asghari-Rad, J.W. Bae, H.S. Kim, Fine tuning of tensile properties in CrCoNi medium entropy alloy through cold rolling and annealing, Intermetallics 113 (2019) 106578, https://doi.org/10.1016/j.intermet.2019.106578.
[16] B. Schuh, R. Pippan, A. Hohenwarter, Tailoring bimodal grain size structures in nanocrystalline compositionally complex alloys to improve ductility, Mater Sci Eng A 748 (2019) 379–385, https://doi.org/10.1016/j.msea.2019.01.073.
[17] P. Sathiyamoorthi, J. Moon, J.W. Bae, P. Asghari-Rad, H.S. Kim, Superior cryogenic tensile properties of ultrafine-grained CoCrNi medium-entropy alloy produced by high-pressure torsion and annealing, Scripta Mater. 163 (2019) 152–156, https://doi.org/10.1016/j.scriptamat.2019.01.016.
[18] L. Rémy, The interaction between slip and twinning systems and the influence of twinning on the mechanical behavior of fcc metals and alloys, Metall. Trans. A 12 (1981) 387–408, https://doi.org/10.1007/BF02648536.

[19] J.K. Mackenzie, Second paper on statistics associated with the random disorientation of cubes, Biometrika 45 (1958) 229–240, https://doi.org/10.2307/2333253.
[20] M. Naeem, H. He, S. Harjo, T. Kawasaki, W. Lin, J.-J. Kai, Z. Wu, S. Lan, X.-L. Wang, Temperature-dependent hardening contributions in CrFeCoNi high-entropy alloy, Acta Mater. 221 (2021) 117371, https://doi.org/10.1016/j.actamat.2021.117371.
[21] H. Fujita, S. Ueda, Stacking faults and f.c.c. (γ) → h.c.p. (ϵ) transformation in 18/8-type stainless steel, Acta Metall. 20 (1972) 759–767, https://doi.org/10.1016/0001-6160(72)90104-6.
[22] J.W. Brooks, M.H. Loretto, R.E. Smallman, Direct observations of martensite nuclei in stainless steel, Acta Metall. 27 (1979) 1839–1847, https://doi.org/10.1016/0001-6160(79)90074-9.
[23] J.W. Brooks, M.H. Loretto, R.E. Smallman, In situ observations of the formation of martensite in stainless steel, Acta Metall. 27 (1979) 1829–1838, https://doi.org/10.1016/0001-6160(79)90073-7.
[24] L. Rémy, Kinetics of strain-induced fcc→hcp martensitic transformation, Metall. Trans. A 8A (1977) 253–258, https://doi.org/10.1007/BF02661637.
[25] G.I. Taylor, Plastic strain in metals, J. Inst. Met. 62 (1938) 307–324.
[26] R. Wang, C. Lu, K.A. Tieu, A.A. Gazder, Slip system activity and lattice rotation in polycrystalline copper during uniaxial tension, J. Mater. Res. Technol. 18 (2022) 508–519, https://doi.org/10.1016/j.jmrt.2022.02.110.
[27] B.E. Warren, X-Ray Diffraction, 1990.
[28] M. Naeem, H. He, F. Zhang, H. Huang, S. Harjo, T. Kawasaki, B. Wang, S. Lan, Z. Wu, F. Wang, Y. Wu, Z. Lu, Z. Zhang, C.T. Liu, X.-L. Wang, Cooperative deformation in high-entropy alloys at ultralow temperatures, Sci. Adv. 6 (2020), https://doi.org/10.1126/sciadv.aax4002 eaax4002.
[29] M. Naeem, H. He, S. Harjo, T. Kawasaki, F. Zhang, B. Wang, S. Lan, Z. Wu, Y. Wu, Z. Lu, C.T. Liu, X.-L. Wang, Extremely high dislocation density and deformation pathway of CrMnFeCoNi high entropy alloy at ultralow temperature, Scripta Mater. 188 (2020) 21–25, https://doi.org/10.1016/j.scriptamat.2020.07.004.
[30] R.P. Reed, R.E. Schramm, Relationship between stacking-fault energy and x-ray measurements of stacking-fault probability and microstrain, J. Appl. Phys. 45 (1974) 4705–4711, https://doi.org/10.1063/1.1663122.
[31] W.G. Nöhring, W.A. Curtin, Cross-slip of long dislocations in FCC solid solutions, Acta Mater. 158 (2018) 95–117, https://doi.org/10.1016/j.actamat.2018.05.027.
[32] E. Oren, E. Yahel, G. Makov, Kinetics of dislocation cross-slip: a molecular dynamics study, Comput. Mater. Sci. 138 (2017) 246–254, https://doi.org/10.1016/j.commatsci.2017.06.039.
[33] D. Hull, D.J. Bacon, Introduction to Dislocations, fifth ed., Butterworth-Heinemann, Oxford, 2011.
[34] Q. Ding, Y. Zhang, X. Chen, X. Fu, D. Chen, S. Chen, L. Gu, F. Wei, H. Bei, Y. Gao, M. Wen, J. Li, Z. Zhang, T. Zhu, R.O. Ritchie, Q. Yu, Tuning element distribution, structure and properties by composition in high-entropy alloys, Nature 574 (2019) 223–227, https://doi.org/10.1038/s41586-019-1617-1.
[35] B. Gludovatz, A. Hohenwarter, K.V.S. Thurston, H. Bei, Z. Wu, E.P. George, R. O. Ritchie, Exceptional damage-tolerance of a medium-entropy alloy CrCoNi at cryogenic temperatures, Nat. Commun. 7 (2016) 1–8, https://doi.org/10.1038/ncomms10602.
[36] M. Yang, L. Zhou, C. Wang, P. Jiang, F. Yuan, E. Ma, X. Wu, High impact toughness of CrCoNi medium-entropy alloy at liquid-helium temperature, Scripta Mater. 172 (2019) 66–71, https://doi.org/10.1016/j.scriptamat.2019.07.010.
[37] W. Woo, J.S. Jeong, D.K. Kim, C.M. Lee, S.H. Choi, J.Y. Suh, S.Y. Lee, S. Harjo, T. Kawasaki, Stacking Fault energy analyses of additively manufactured stainless steel 316L and CrCoNi medium entropy alloy using in situ neutron diffraction, Sci. Rep. 10 (2020) 2–4, https://doi.org/10.1038/s41598-020-58273-3.
[38] Y. Liu, Y. He, S. Cai, Gradient recrystallization to improve strength and ductility of medium-entropy alloy, J. Alloys Compd. 853 (2021) 157388, https://doi.org/10.1016/j.jallcom.2020.157388.
[39] S. Yoshida, T. Bhattacharjee, Y. Bai, N. Tsuji, Friction stress and Hall-Petch relationship in CoCrNi equi-atomic medium entropy alloy processed by severe plastic deformation and subsequent annealing, Scripta Mater. 134 (2017) 33–36, https://doi.org/10.1016/j.scriptamat.2017.02.042.
[40] W. Woo, Y.S. Kim, H.B. Chae, S.Y. Lee, J.S. Jeong, C.M. Lee, J.W. Won, Y.S. Na, T. Kawasaki, S. Harjo, K. An, Competitive strengthening between dislocation slip and twinning in cast-wrought and additively manufactured CrCoNi medium entropy alloys, Acta Mater. 246 (2023), https://doi.org/10.1016/j.actamat.2023.118699.
[41] O. Muránsky, L. Balogh, M. Tran, C.J. Hamelin, J.S. Park, M.R. Daymond, On the measurement of dislocations and dislocation substructures using EBSD and HRSD techniques, Acta Mater. 175 (2019) 297–313, https://doi.org/10.1016/J.ACTAMAT.2019.05.036.
[42] M.F. Ashby, The deformation of plastically non-homogeneous materials, Philos. Mag. A 21 (1970) 399–424, https://doi.org/10.1080/14786437008238426.